Schimmerling, Science **174**, 1127 (1971).
[18]K. G. Vosburgh, Science **174**, 1125 (1971).
[19]C. A. Tobias and P. Todd, Nat. Cancer Inst. Monogr. **24**, 1 (1966).
[20]V. P. Bond and G. M. Tjlislar-Lentulis, in *Elementary Particles: Science, Technology and Society* (Academic, New York, 1971), p. 241.

PHYSICAL REVIEW B VOLUME 7, NUMBER 7 1 APRIL 1973

Electronic Raman Effect and Spectroscopic Studies of $NdAlO_3$†

E. Finkman* and E. Cohen
Department of Physics, Technion-Israel Institute of Technology, Haifa, Israel

L. G. Van Uitert
Bell Laboratories, Murray Hill, New Jersey 07974

(Received 21 September 1972)

The electronic excitations of the ground ^4I term of Nd^{3+} in the trigonal phase of $NdAlO_3$ have been studied. All the 26 energy levels of this term were measured by means of Raman scattering, fluorescence, and optical absorption in the visible region and the near infrared. According to the irreducible representations of D_3—the site symmetry of Nd^{3+} in this crystal—these levels were classified by polarization selection rules. The observed levels were analyzed within the framework of crystal field theory. It was found that in order to obtain a best fit to the Stark splitting, J mixing between all multiplets of the ^4I term had to be included. The six crystal field parameters thus obtained yielded a mean standard deviation of 6.6 cm^{-1} between the measured and calculated energy levels. Using the eigenvectors of the energy states that were obtained by the crystal field calculations the g factors and relative electronic Raman intensities were computed. An asymmetry is predicted in the xz and zx electronic Raman spectra as observed experimentally. However, the agreement between calculated and measured values for both g factors and relative Raman intensities is qualitative only. The discrepancies are too large to account for by experimental errors only. Two factors are proposed as a possible explanation: (a) the ion-lattice interaction in the ground $^4I_{9/2}$ multiplet, which modifies the eigenvectors; (b) the proximity of the exciting laser line to Nd^{3+} states might introduce near-resonance effects which will influence the relative Raman intensities.

I. INTRODUCTION

The electronic Raman effect of rare-earth ions in crystals has been studied during the last years, both theoretically[1–3] and experimentally.[4–6] Within the framework of crystal field theory the electronic-polarizability tensor can be calculated. The relative strength of the expected Raman lines can be computed from it and compared with the observed transitions. Such an analysis, combined with energy levels and magnetic g-factor calculation, can be used to examine crystal field models. This approach has been applied to the cases of Ce^{3+} in $CeCl_3$[4] and Dy^{3+} in dysprosium garnets.[5]

$NdAlO_3$ belongs to a group of rare-earth aluminates (La, Ce, Pr, and Nd), which have D_{3d}^6 symmetry at room temperature.[7–11] All these crystals undergo a trigonal-to-cubic (perovskite) transition at high temperature. Interesting behavior is observed in $PrAlO_3$, which has two additional phase transitions below room temperature,[12] which are attributed to an interaction between the crystal vibrations and the electronic excitations of the Pr^{3+} ion.[13,14] Since $NdAlO_3$ does not have any phase transition (magnetic or structural) down to 2 °K, the electronic structure of the Nd^{3+} ion in this crystal and its interaction with the lattice vibrations can be contrasted with those of $PrAlO_3$. From the results of this study on $NdAlO_3$ we conclude that there is a pronounced ion-phonon interaction in the $^4I_{9/2}$ ground multiplet of Nd^{3+}, which, however, is insufficient to induce a phase transformation.

This paper describes a study of the ^4I term of Nd^{3+} in $NdAlO_3$. All the electronic levels of this term were observed experimentally by Raman scattering and infrared absorption or fluorescence and their symmetry determined from the polarization selection rules. A crystal field analysis was applied to the results and relative scattering intensities were calculated.

In Sec. II we review the crystal field theory applied to the electronic Raman effect. The experimental procedure and results are given in Sec. III. An analysis of these results is presented in Sec. IV.

II. CRYSTAL FIELD THEORY AND ELECTRONIC RAMAN EFFECT

The site symmetry of the Nd^{3+} ion in $NdAlO_3$ is D_3. However, the spectroscopic study indicates that the deviation from cubic (O_h) symmetry is very

small. In consequence, all the Γ_5^- levels of the cubic field[15] split into pairs of closely spaced levels of D_3 symmetry types, Γ_4 and $\Gamma_{5,6}$ under the influence of the small trigonal distortion.

Polarization selection rules for electric dipole transitions (in absorption and fluorescence) are used in order to identify the Stark levels. For the case of an ion with odd number of electrons in D_3 symmetry these are as follows: $\Gamma_4 \rightarrow \Gamma_4(\sigma, \pi)$, $\Gamma_4 \rightarrow \Gamma_{5,6}(\sigma)$, and $\Gamma_{5,6} \rightarrow \Gamma_{5,6}(\pi)$.

As some of the observed transitions appear in both σ and π polarizations in spectra that were taken at 2 °K it is concluded that the Nd^{3+} ground state is of Γ_4-symmetry type. We shall denote it by $^4I_{9/2}(\Gamma_4^a)$. For absorption at very low temperatures we expect to observe transitions only from this state. Thus, transitions to all excited states are allowed in σ polarization and only transitions to Γ_4-type excited states in π polarization.

The energy levels, Zeeman-splitting factors, and relative electronic Raman intensities have been calculated within the framework of crystal field theory. Following Wybourne[16] the crystal field perturbation is given by

$$V_c = \sum_{k,q} B_q^k C_q^{(k)} . \tag{1}$$

For the f^N configuration, the matrix elements of V_c are given by

$$(f^N\gamma SLJM|\, V_c \,|f^N\gamma' SL'J'M') = \sum_{k,q} B_q^k (-1)^{J-M} \begin{pmatrix} J & k & J' \\ -M & q & M' \end{pmatrix} \times (f\|\, C^{(k)} \,\|f)(f^N\gamma SLJ\|\, U^{(k)} \,\|f^N\gamma' SL'J') , \tag{2}$$

where

$$(f^N\gamma SLJ\|\, U^{(k)} \,\|f^N\gamma' SL'J') = (-1)^{S+L+J'+k}[(2J+1)(2J'+1)]^{1/2} \times \begin{Bmatrix} J & J' & k \\ L' & L & S \end{Bmatrix} (f^N\gamma SL\|\, U^{(k)} \,\|f^N\gamma' SL') . \tag{3}$$

The reduced matrix elements $(SL\|\, U^{(k)} \,\|SL')$ were calculated by Nielson and Koster.[17]

Symmetry considerations for D_3 site symmetry of the Nd^{3+} ion in the crystal lead to a potential V_c of the form

$$V_c = B_0^2 C_0^{(2)} + B_0^4 C_0^{(4)} + B_3^4 (C_{-3}^{(4)} - C_3^{(4)}) + B_0^6 C_0^{(6)} + B_3^6 (C_{-3}^{(6)} - C_3^{(6)}) + B_6^6 (C_{-6}^{(6)} + C_6^{(6)}) . \tag{4}$$

The scattering tensor for the electronic Raman effect is given by[4]

$$P(f, g;\ \nu, \epsilon_\rho, \epsilon_\sigma) = P_S + P_A = e^2 \sum_i \left(\frac{E_i}{(E_i - h\nu)(E_i + h\nu)} [(f|\, r_\sigma \,|i)(i|\, r_\rho \,|g) + (f|\, r_\rho \,|i)(i|\, r_\sigma \,|g)] + \frac{h\nu}{(E_i - h\nu)(E_i + h\nu)} [(f|\, r_\sigma \,|i)(i|\, r_\rho \,|g) - (f|\, r_\rho \,|i)(i|\, r_\sigma \,|g)] \right), \tag{5}$$

where g, i, f are the ground, intermediate, and final states, respectively; ν is the exciting laser frequency; E_i is the energy of the ith intermediate state; ϵ_ρ is the polarization of the incident (laser) beam; and ϵ_σ is the polarization of the scattered light. The second term in (5) transforms like an axial vector and is antisymmetric in the indices ρ and σ. As a result

$$P(f, g;\ \nu, \epsilon_\sigma, \epsilon_\rho) = P_S + P_A ,$$

while (6)

$$P(f, g;\ \nu, \epsilon_\rho, \epsilon_\sigma) = P_S - P_A .$$

As the intensity of the scattered radiation is proportional to P^2, there can be an asymmetry between the scattered intensities for $\rho\sigma$ and $\sigma\rho$ polarizations. The magnitude of this asymmetry depends both on the ratio $h\nu/E_i$ and on the relative values of the symmetric and antisymmetric terms that appear in Eq. (5).

Axe[1] treated the problem of calculating the elements of the scattering tensor by employing the closure relations of Judd[18] and Ofelt[19] for the sum over the intermediate states. He showed that the components of the scattering tensor $(\alpha_{\rho\sigma})_{gf}$ can be expressed as linear combinations of elements of the irreducible tensors of rank 0, 1, and 2 between the final and initial electronic states. Equations (2)–(5) of Axe[1] give explicit expressions for the transformation of the scattering tensor from the irreducible spherical-tensor coordinates to the complex Cartesian basis: $x_0 = z$; $x_+ = (1/\sqrt{2})(x + iy)$; $x_- = (1/\sqrt{2})(x - iy)$. Usually we are interested in the transformation between the components $\alpha_q^{(k)}$ of the polarizability tensor in the irreducible basis and $\alpha_{\rho\sigma}$, the polarizability in real rectilinear coordinates. This is given in the Appendix together with symmetry considerations for calculating the relative intensities in trigonal symmetry.

We have computed the matrix elements of the form

$$(f^3\gamma SLJM|\, \alpha_q^{(k)} \,|f^3\gamma' SL'J'M')$$

$$= \alpha_k'(\nu)\left[(-1)^{J-M}\begin{pmatrix} J & k & J' \\ -M & q & M' \end{pmatrix} \times (f^3\gamma SLJ \| U^{(k)} \| f^3\gamma' SL'J')\right], \quad k=0,1,2 \qquad (7)$$

for the transitions within $^4I_{9/2}$ and between this term and $^4I_{11/2}$. The reduced matrix elements are given by Eq. (3) and are tabulated in Ref. 17 for $k=2$. For $k=1$ we get the expression[20]

$$(l^N\gamma SL \| U^{(1)} \| l^N\gamma' SL') = \delta(L,L')\delta(\gamma,\gamma')\left(\frac{L(L+1)(2L+1)}{l(l+1)(2l+1)}\right)^{1/2} . \qquad (8)$$

The result for $k=0$ is

$$[f(l^N)|\alpha_0^{(0)}|g(l^N)] = 3\alpha_0'\delta(f,g)/(2l+1)^{1/2} \qquad (9)$$

and it can be seen that $\alpha_0^{(0)}$ does not contribute to the electronic Raman transitions. Similar results were given in some detail by Mortensen and Koningstein.[2,3]

To calculate the transition probabilities one still needs to know the matrix elements $(4f|r|n', l\pm1)$ and the energies $E_{(n',l\pm1)}$ for all the excited configurations. Assuming spherical symmetry, the only nonzero matrix elements are those contributed by the $4f^{n-1}5d$ and $4f^{n-1}5g$ excited configurations.

Thus, Axe expresses the factors $\alpha_k'(\nu)$ $(k=1, 2)$ as follows:

$$\alpha_1'(\nu) \cong e^2\left(\frac{2^3\cdot 3}{7}\right)^{1/2}\left(\frac{h\nu(4f|r|5d)^2}{(E_{5d}-h\nu)(E_{5d}+h\nu)} - \frac{h\nu(4f|r^2|4f)}{(E_{5g}-h\nu)(E_{5g}+h\nu)}\right), \qquad (10)$$

$$\alpha_2'(\nu) \cong e^2\left[\left(\frac{2^3\cdot 3^2}{5\cdot 7}\right)^{1/2}\frac{E_{5d}(4f|r|5d)^2}{(E_{5d}-h\nu)(E_{5d}+h\nu)} + \left(\frac{2^3\cdot 5}{3^2\cdot 7}\right)^{1/2}\frac{E_{5g}(4f|r^2|4f)}{(E_{5g}-h\nu)(E_{5g}+h\nu)}\right].$$

The radial integrals $(4f|r|5d)^2$ and $(4f|r|5g)^2$ [which is approximated here by $(4f|r^2|4f)$] can be estimated by interpolating between Rajnak's[21] values for Pr^{3+} and Tm^{3+}. Also, the energies of the excited configurations can be estimated from the free-ion spectrum. However, these values might change significantly for Nd^{3+} in a crystal. It is worth noting that by fitting the results of Faraday rotation experiments[22] for $NdAlO_3$ it has been shown that the only considerable contribution comes from the $4f^25d$ configuration. Its effective energy was calculated to be $E_{5d}=42\,700$ cm^{-1}. This value is smaller than the center of gravity of the free-ion $4f^25d$ configuration and is also too small to account for the electronic Raman intensity as discussed in Sec. IV.

Now the electronic states of the Nd^{3+} in the crystal are given by linear combinations of $|JM)$'s,

$$|\psi) = \sum_{J,M} a(JM)|\gamma JM) .$$

The Raman scattering tensor for a transition between the levels g and f is then given by

$$(\alpha_{\rho\sigma})_{gf} = (f|\alpha_{\rho\sigma}|g) = \sum a^*(J'M')a(JM)(\gamma'SL'J'M'|\alpha_{\rho\sigma}|\gamma SLJM) . \qquad (11)$$

The eigenvectors [i.e., the expansion coefficients $a(JM)$] are obtained from crystal field calculations. The relative intensities of the Raman scattering might be used as a test of the applicability of the crystal field model.

III. EXPERIMENTAL PROCEDURE AND RESULTS

Both Raman scattering and fluorescence spectra were excited using the 4880-Å line of an Ar^+ laser with 250-mW total output. In order to distinguish Raman scattering from fluorescence the spectrum was also observed with excitation by the 5145-Å line of Ar and by the 6328-Å line of He-Ne laser (45 mW). The light was passed through a spex 1400 double monochromator equipped with a cooled photomultiplier (ITT FW 130). The signal was amplified using a dc electrometer (Victoreen 1001). Infrared absorption spectra were taken with a Perkin–Elmer 210 monochromator and a PbS detector. The signal was chopped and amplified using PAR HR-8 lock-in amplifier.

Two oriented crystals of $NdAlO_3$ were used. The crystals were $2.5\times3\times5$ mm^3 and $0.1\times2\times2$ mm^3 in dimension. Spectra were taken on several crystals, some not oriented in order to check the sample dependence.[23]

The sample was mounted in a stainless-steel Dewar. The temperature, within a range of 5–300 °K, was maintained by flowing cold He gas over the sample and controlled using a feedback system.[24]

Absorption from all the crystal field components of the ground-state multiplet could be obtained by raising the temperature to the order of $\sim E_n/k$ or higher. We introduce this in Figs. 1 and 2 for transitions to $^2P_{1/2}$ and $^4F_{3/2}$. In our notation a, b, c, ... denote the order in which the Stark components of each symmetry type appear within a term. We find only four components in the $^4I_{9/2}$ multiplet instead of the expected five. However, the polarization of the highest observed component of the ground state (at 595 cm^{-1}) indicates that it is an unresolved quartet consisting of Γ_4 and $\Gamma_{5,6}$ states. This can be seen from the room-temperature absorption spectrum $^4I_{9/2}-{}^4F_{3/2}$ (shown in Fig. 2). The transitions from the three lowest Stark components of $^4I_{9/2}$ to $^4F_{3/2}(\Gamma_{5,6})$ are strictly polarized, while that originating at the 595 cm^{-1} level appears in both σ and π polarizations. Since

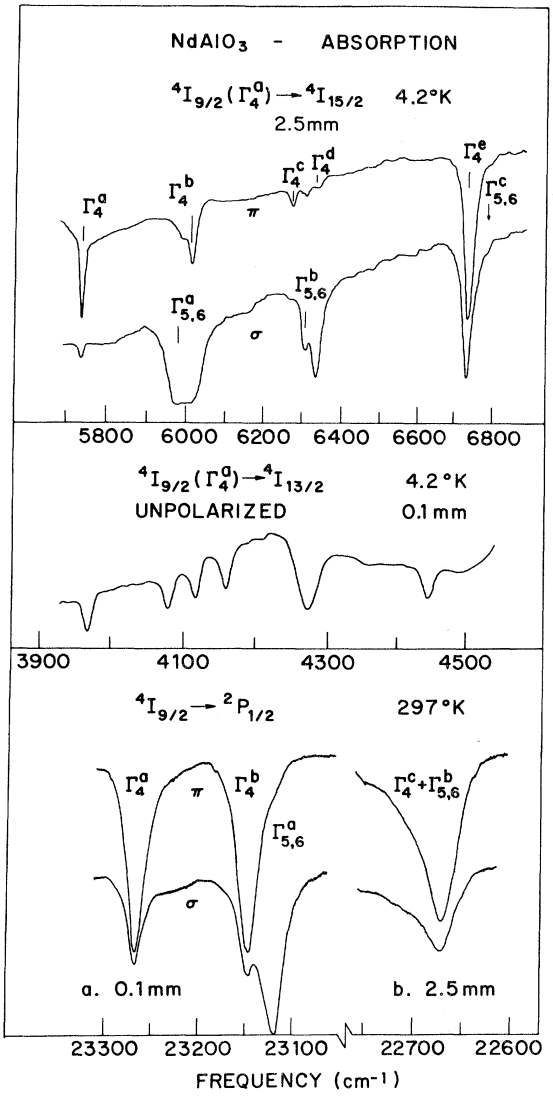

FIG. 1. Absorption to $^4I_{13/2}$ and $^4I_{15/2}$ at 2 °K and absorption to $^2P_{1/2}$ at elevated temperatures showing all the components of $^4I_{9/2}$.

the selection rules indicate that a transition to a $\Gamma_{5,6}$ level can occur in only one polarization, it is concluded that the level at 595 cm^{-1} is an unresolved $\Gamma_4+\Gamma_{5,6}$. This was further verified by fluorescence and Raman studies.

The spectral lines corresponding to transitions from the ground state $^4I_{9/2}(\Gamma_4^a)$ to the $^4I_{13/2}$ and $^4I_{15/2}$ multiplets in the near infrared region are shown in the two upper parts of Fig. 1. Six out of the seven expected lines of the $^4I_{13/2}$ spectrum are observed. However, the examination of the polarized spectra indicates that the strong line near 4280 cm^{-1} consists of two unresolved Kramers doublets $(\Gamma_4^d+\Gamma_{5,6}^b)$. Similarly, only seven out of the eight expected lines are observed in the $^4I_{15/2}$ spectrum. The position of the missing line, corresponding to the transition $^4I_{9/2}(\Gamma_4^a)\rightarrow{}^4I_{15/2}(\Gamma_{5,6}^c)$, was determined from the appearance of two additional absorption lines from the excited Γ_4^b and $\Gamma_{5,6}^a$ states of $^4I_{9/2}$ (at 122 and 148 cm^{-1}, respectively) at 77 °K. Such a pair accompanies each of the spectral lines observed at 4.2 °K. However, an extra pair of observed lines is due to the transitions from $^4I_{9/2}(\Gamma_4^b)$ and $\Gamma_{5,6}^a$ to $^4I_{15/2}(\Gamma_{5,6}^c)$. The expected position of this level is indicated by an arrow in Fig. 1.

The α polarization (propagation of the light beam parallel to the c axis) of all the spectra taken in both the visible and infrared regions is very similar to the σ polarization. This indicates that all transitions are of electric dipole character.

The fluorescence spectrum of $NdAlO_3$ is complicated, because Nd^{3+} tends to emit from many different levels. Broad-band (1000–5000 cm^{-1}) excitation in the region of 20000–25000 cm^{-1} resulted in a very broad and intense fluorescence. To overcome this we selected a single emitting level by using the laser light as an excitation source. The best fluorescing level for this purpose proved to be the $^4G_{7/2}$ lower component, at about 5266 Å, excited with the 5145-Å Ar^+-laser line. Fluorescence spectra from this level to the $^4I_{9/2}$ and $^4I_{11/2}$ multiplets are represented in Figs. 3 and 4. Two interesting phenomena may be noted in Fig. 4. First, the absorption coefficient for the transition $^4I_{9/2}(\Gamma_4^a)\rightarrow{}^4G_{7/2}(\Gamma_4^a)$ is so large that this fluorescence line is totally absorbed, even though the crystal was only 0.1 mm thick. Second, in addition to fluorescence from the lower level of the $^4G_{7/2}$ into the ground-state multiplet, lines corresponding to transitions from other Stark components of $^4G_{7/2}$ to the $^4I_{9/2}(\Gamma_{5,6}^a)$ level are also observed even at 2 °K. The separation between these components of $^4G_{7/2}$ is about 45 cm^{-1}, as can be seen in the fluorescence spectrum in Fig. 3. Thermalization between these levels must, therefore, be slow relative to the radiative decay. This is probably due to the fact that the density of phonon states at 45 cm^{-1} is small, as suggested by the vibronic spectrum near the $^4I_{9/2}(\Gamma_4^a)\rightarrow{}^2P_{1/2}$ transition (Fig. 5).

The space group for $NdAlO_3$ is D_{3d}^6 with two molecules per unit cell (at the temperature range from 1.2 to ~1500 °K), with Al ions at C_{3i} sites, Nd ions at D_3 sites, and oxygen ions at C_2 sites. The symmetry division of normal modes for this structure is[10]

$$\Gamma(D_{3d}^6)=\Gamma_1^+ + 3\Gamma_2^+ + 4\Gamma_3^+ + 2\Gamma_1^- + 4\Gamma_2^- + 6\Gamma_3^- .$$

Five of these modes are Raman active: $\Gamma_1^+ + 4\Gamma_3^+$. Polarized Raman spectra at room temperature are shown in Fig. 6, with the usual notation for the polarization (the x and y axes are chosen arbitrarily

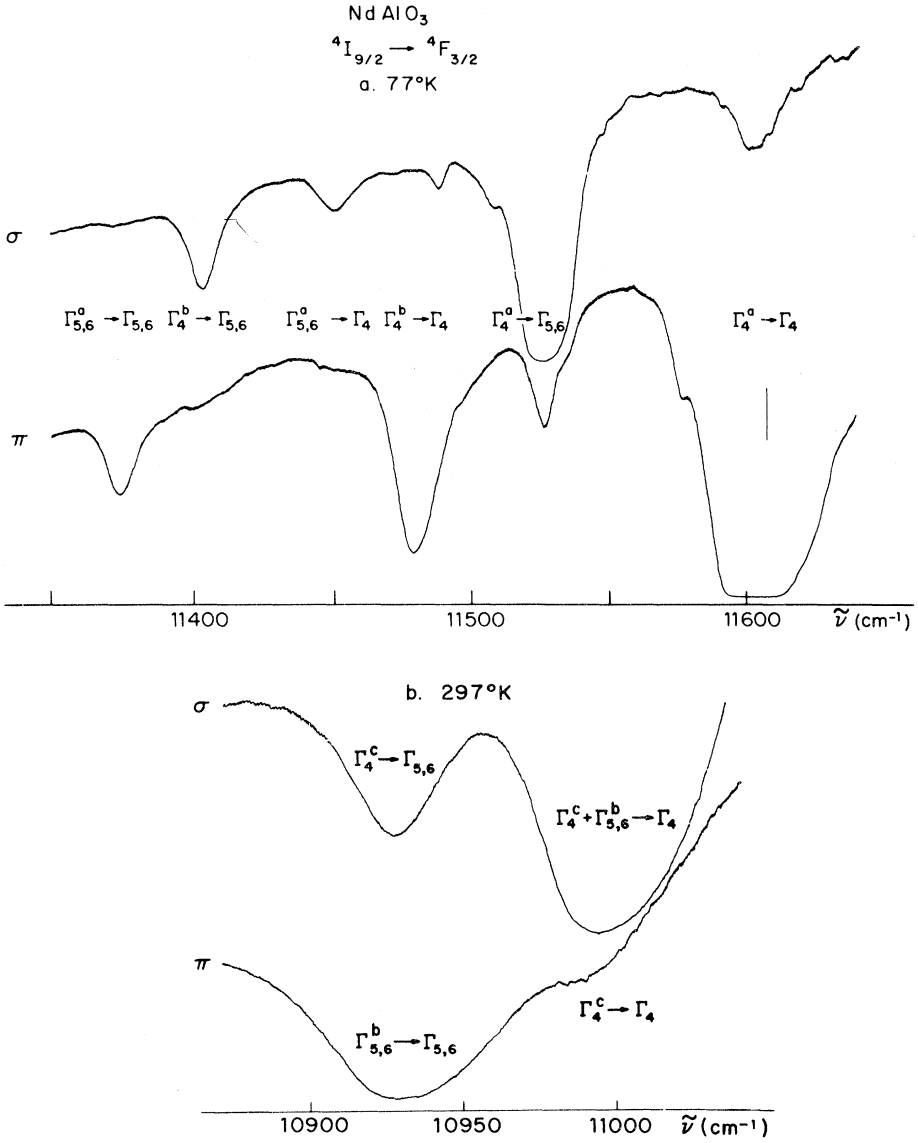

FIG. 2. Absorption to $^4F_{3/2}$ from all the components of $^4I_{9/2}$ at elevated temperatures.

in a plane perpendicular to the $C_3 = z$ axis). According to the selection rules[25] the Γ_1^+ mode has only diagonal elements of the polarizability, and cannot contribute to nondiagonal polarizations. This mode is the only one that contributes to zz polarization. This is clearly presented in Fig. 6, where the Γ_1^+ and three out of four Γ_3^+ modes are observed. The phonon frequencies and relative intensities for the Raman lines in $NdAlO_3$ are given in Table I. The intensities are normalized to that of the Γ_1^+ mode in zz polarization ($I = 100$). Earlier data for this crystal are incomplete,[10,26] mainly because of poor polarization.

Although we do not have the phonon density of states for $NdAlO_3$, we can get some idea of its shape from the vibronic spectrum accompanying the 4300-Å $^4I_{9/2}(\Gamma_4^a) \rightarrow {}^2P_{1/2}$ transition at low temperature (Fig. 5). This vibronic spectrum could be identified only up to about 500 cm^{-1} because of overlapping due to the transitions to the multiplet $^2D_{5/2}$. The lines belonging to these transitions are dashed in Fig. 5.

Raman scattering spectra at 2 °K using the 4880-Å line as an excitation source are shown in Fig. 4. In addition to the phonon lines, transitions to all the crystal field levels of the multiplets $^4I_{9/2}$ and $^4I_{11/2}$ of Nd^{3+} are observed (the electronic lines are marked e). Using the Γ_1^+ phonon line as a measure of the polarization quality of the crystal, we observe that the polarization is incomplete. This property will be discussed further in Sec. IV.

It should be noted that the Raman scattering from all Stark components of the $^4I_{9/2}$ ground multiplet is observed even at room temperature, although the

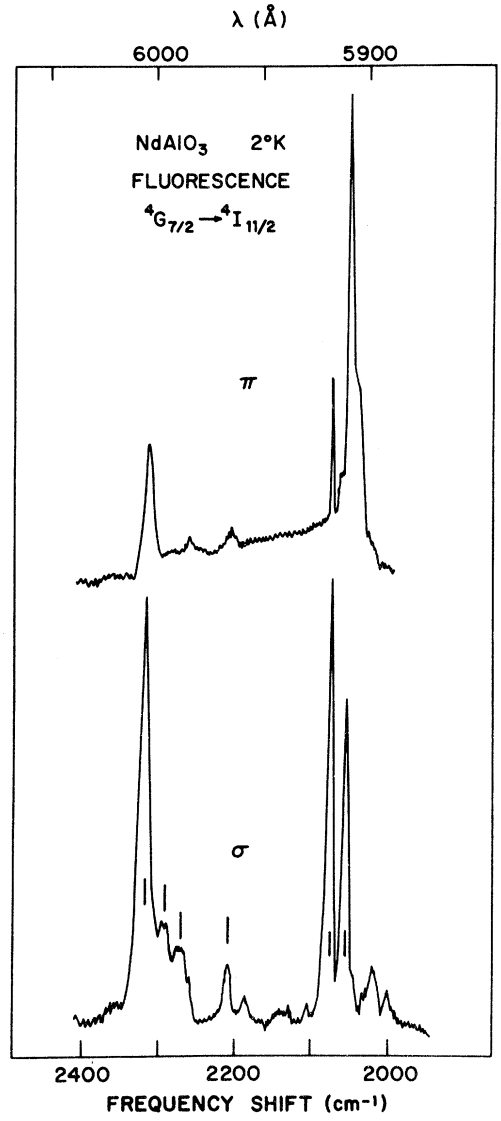

FIG. 3. Fluorescence to $^4I_{11/2}$ from the $^4G_{7/2}$, excited with the 5145-Å line of the Ar^+ laser. The vertical lines in the σ spectrum indicate all the components of $^4I_{11/2}$.

TABLE I. Relative intensities of phonon Raman lines in $NdAlO_3$ normalized to the intensity of the Γ_1^+ transition at zz polarization (underlined). The results at 2 °K are given in parentheses.

Polarization → Energy (cm^{-1})	yy	zz	$xz(yz)$	$zx(zy)$	xy
56 (49) (Γ_3^+)	130	2.5 (39)	130 (120)	120 (110)	100 (120)
166 (168) (Γ_3^+)	10	~0 (0.3)	~0 (1.6)	~0 (0.4)	6 (4)
239 (251) (Γ_1^+)	12	<u>100</u> (<u>100</u>)	5 (1)	1 (40)	~0 (1)
509 (512) (Γ_3^+)	2.5	~0 (0.3)	1 (1.5)	1.5 (1.5)	1.5 (1.5)

lines are very weak (see Fig. 6). An asymmetry between the xz and zy electronic Raman spectra is observed (compare the two first electronic Raman

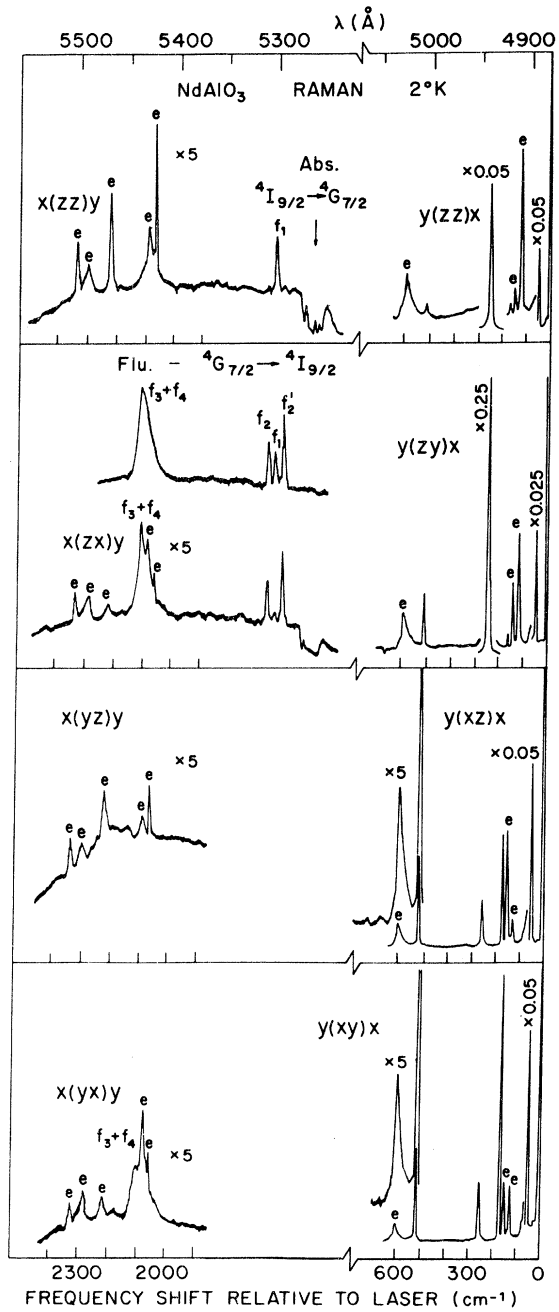

FIG. 4. Polarized Raman spectra of $NdAlO_3$ at 2 °K. Electronic scattering of $^4I_{9/2}$ and $^4I_{11/2}$ multiplets are observed in addition to the phonon scattering. The Raman spectrum of $^4I_{11/2}$ is overlapped by fluorescence $^4G_{7/2} \rightarrow {}^4I_{9/2}$ (inserted for comparison). The lines are designated $f_i (i = 1, \ldots, 4)$ corresponding to the transitions to Γ_4^b, $\Gamma_{5,6}^a$, Γ_4^c, and $\Gamma_{5,6}^b$, respectively. A broad fluorescence band is evidenced by the appearance of absorption lines to $^4G_{7/2}$.

lines). It is more pronounced at room temperature, because of better polarization, than in the low-temperature spectra.

Several experimental difficulties have been encountered in obtaining the Raman scattering of the $^4I_{11/2}$ multiplet at low temperatures. The crystal absorbs slightly the 4880-Å laser line (into the vibronic tail of $^2G_{9/2}$) thus giving rise to two types of fluorescence:

(a) A broad band stretching over most of the visible region. Its strength depends on the point of incidence of the exciting light in the crystal. Such a broad-band fluorescence is often observed in concentrated rare-earth crystals. This is probably due to impurities.

(b) Fluorescence of the Nd^{3+} ion, in particular the transitions $^4G_{7/2} \rightarrow {}^4I_{9/2}$, which overlap the Raman spectrum of $^4I_{11/2}$ (these are marked *f* in Fig. 4).

In order to ascertain our identification, we have depicted in Fig. 4 the fluorescence spectrum excited by the 5145-Å Ar line. The broad-band fluorescence is evidenced by the appearance of the absorption lines from $^4I_{9/2}(\Gamma_4^a)$ to all components of the $^4G_{7/2}$ multiplet. Raman spectra excited by the 6328-Å He-Ne line gave similar results for $^4I_{9/2}$. The scattering to $^4I_{11/2}$ was too weak to be observed. It was impossible to obtain a better Raman spectrum of the $^4I_{11/2}$ multiplet by using the 5145-Å Ar^+ line because this spectrum is totally absorbed by the $^2G_{7/2}$ and $^4G_{5/2}$ multiplets near 5800 Å.

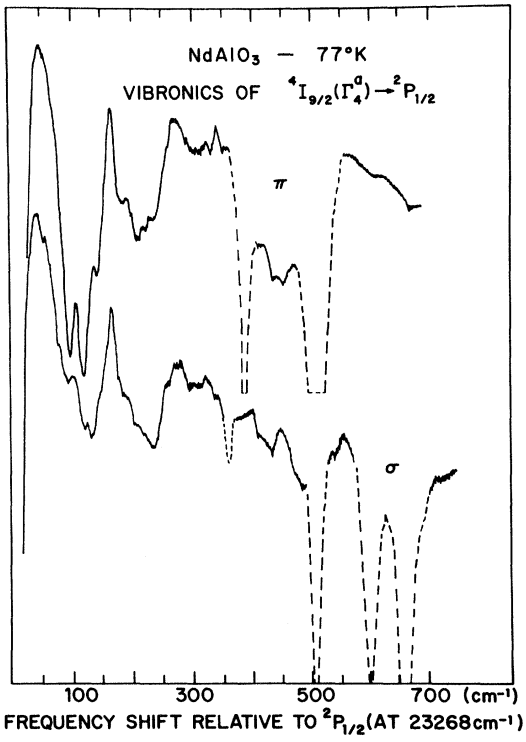

FIG. 5. Vibronics associated with the $^4I_{9/2}(\Gamma_4^a) \rightarrow {}^2P_{1/2}$ transition. (The dashed spectral lines are due to the transitions $^4I_{9/2} \rightarrow {}^2D_{5/2}$.)

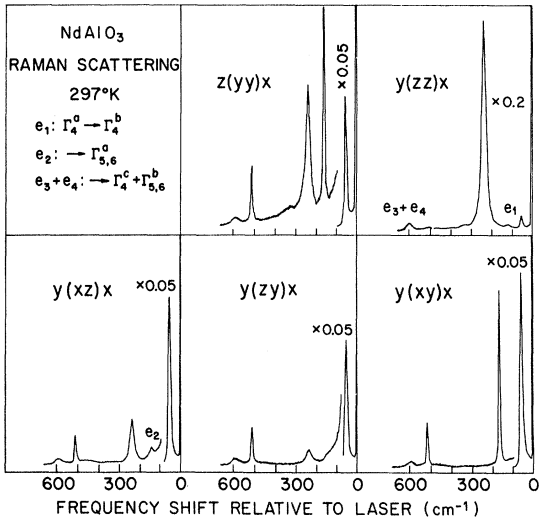

FIG. 6. Polarized Raman spectra of $NdAlO_3$ at room temperature. In addition to the phonon lines, weak lines (e_i) corresponding to electronic transitions of Nd^{3+} are observed.

IV. ANALYSIS AND CONCLUSIONS

A. Energy Levels and *g* Factors

All the observed energy levels of the ^4I ground term (26 levels) were used to obtain the crystal field parameters of Eq. (4). The mathematical iterative methods of fitting the best crystal field parameters are sometimes sensitive to the initial values chosen for these parameters (such is the case for dysprosium garnets discussed by Wadsac *et al.*[5]). In order to overcome this problem two important observations were used in obtaining the correct crystal field parameters: (i) The order of magnitude and sign of B_0^2 were determined from the splitting of $^4F_{3/2}$ and $^2P_{3/2}$ at 4.2 °K. The crystal field Hamiltonian for a $J = \frac{3}{2}$ multiplet is $V_c = B_0^2 C_0^{(2)}$ and thus B_0^2 can be determined directly from this splitting. The corresponding values of B_0^2 are -475 ± 3 cm^{-1} and -600 ± 5 cm^{-1} for $^4F_{3/2}$ and $^4P_{3/2}$, respectively. (ii) Since the level splittings are very close to those expected for O_h symmetry, the ratios of the parameters B_3^4/B_0^4 and $B_q^6/B_0^6 (q = 3, 6)$ are expected to obey the cubic relationships[27] listed in Table II.

The search for a set of crystal field parameters is done by using a nonlinear least-square fit programmed for a computer.[28] At first, the calculations were done using first-order perturbation

TABLE II. Comparison between the observed ratios of the crystal field parameters in $NdAlO_3$ and those expected for cubic symmetry.

	$\frac{B_3^4}{B_0^4}$	$\frac{B_3^6}{B_0^6}$	$\frac{B_6^6}{B_0^6}$	B_0^2 (cm^{-1})
Cubic	−1.195	0.605	0.634	0.0
Set A	−1.51	0.541	0.569	−793.6
Set B	−0.92	0.603	0.624	−530.4

theory, neglecting J mixing. The parameters obtained in this way and the mean standard deviation for the calculated energies are given in Table III, column A. The large mean deviation of 16.5 cm^{-1} is attributed to the neglect of the interaction between the J multiplets. Then the matrix elements connecting the states of all J's of the ^4I term were added to the energy matrix in order to improve the fit. The energy levels are calculated for each J multiplet around its center of gravity, while the energy separations between the four ^4I_J multiplets were added by including the spin-orbit interaction in the Hamiltonian. This interaction was included in the form[29] $H_{SO} = \sum_{n=1}^{3} \lambda_n (\vec{L} \cdot \vec{S})^n$. The parameters which best fitted the multiplet separations were: $\lambda_1 = 294.02$ cm^{-1}, $\lambda_2 = 2.45$ cm^{-1}, and $\lambda_3 = 0.04$ cm^{-1}. The results of the best-fitted parameters for the crystal field Hamiltonian including the J mixing are given in column B of Table III. Not only is the standard deviation much reduced, but the values of the parameters are much closer to those expected for cubic symmetry. The comparison between the observed ratios of the crystal field parameters in $NdAlO_3$ and those expected for cubic symmetry is given in Table II. The only substantial difference between the parameters of column B and those expected for cubic symmetry is the appearance of the parameter B_0^2, which is relatively large. It is interesting to mention that B_0^2 for both $^4F_{3/2}$ and $^2P_{3/2}$ decreases by 15% between 77 °K and room temperature. A similar change in the splitting was observed for $^2D_{5/2}$, but not for any one of the multiplets of ^4I. This can be explained by the relative magnitude of $B_q^6(q = 0, 3, 6)$ which occurs in V_c for $J \geq 3$. These parameters are the largest in V_c, thus the changes in B_0^2 do not greatly affect the crystal field splitting of multiplets with $J \geq 3$.

TABLE III. Crystal field parameters B_q^k for the ^4I term of Nd^{3+} in $NdAlO_3$; column A: a fit without J mixing, and column B: a fit including J mixing.

Parameter	A (cm^{-1})	B (cm^{-1})
B_0^2	−793.6	−530.4
B_0^4	1021.4	490.3
B_3^4	−678.8	−449.4
B_0^6	−1691.3	−1646.9
B_3^6	−916.3	−992.0
B_6^6	−963.3	−1026.6
Mean standard deviation	16.5	6.6

We calculated the energy levels and their associated g factors for the term ^4I of Nd^{3+} in $NdAlO_3$, using the parameters of Table III, column B. The results are given in Table IV, together with the observed energy levels and the $g_{\parallel}$ factors of the three lowest levels. Classification of the states is also given according to irreducible representations of D_3, as was determined by polarization studies. The fit between the measured and calculated energy levels is good, but there are discrepancies between the measured and calculated g factors. We did not succeed in trying to improve the fit between the observed and calculated g factors by changing the values of the crystal field parameters. Changes of the B_q^k's affected the values of the calculated energy levels much more than they did for those of the g factors. Thus, a fit for both the energy levels and the g factors could not be achieved simultaneously.

TABLE IV. Energy levels and associated g factors for ^4I ground term of Nd^{3+} in $NdAlO_3$. The calculations were made by using the parameters of Table III, column B.

J multiplet	Γ_i assignment	Expt. Energy (cm^{-1})	Expt. $g_{\parallel}$	Calc. Energy (cm^{-1})	Calc. $g_{\parallel}$	Calc. $g_{\perp}$
	4	0	1.06	−1.3	1.26	3.17
	4	122	2.10	125	3.48	1.67
$\frac{9}{2}$	5,6	148	2.10	146	3.03	
	4	595		591	2.40	0.90
	5,6	595		599	3.23	
	4	2056		2049	0.53	4.39
	5,6	2078		2082	4.06	
	4	2212		2208	4.16	2.91
$\frac{11}{2}$	5,6	2278		2290	4.41	
	4	2295		2299	4.88	1.92
	4	2321		2313	8.29	0.25
	4	3968		3966	2.25	5.45
	5,6	4080		4080	0.11	
	4	4117		4116	6.00	3.14
$\frac{13}{2}$	4	4159		4150	6.35	1.05
	5,6	4274		4279	6.79	
	4	4278		4281	0.86	2.29
	4	4442		4441	7.08	5.00
	4	5738		5740	4.46	7.28
	5,6	5977		5996	3.16	
	4	6021		6019	7.66	0.85
	4	6273		6260	3.53	6.88
$\frac{15}{2}$	4	6309		6303	7.35	3.97
	5,6	6336		6335	8.30	
	4	6737		6734	4.47	8.03
	5,6	6761		6765	13.00	

TABLE V. Selection rules for electronic Raman scattering for an ion with an odd number of electrons for D_3 and C_{3v} symmetries. $S_x=\alpha^A_{yz}-\alpha^A_{zy}$, $S_y=\alpha^A_{zz}-\alpha^A_{xz}$, $S_z=\alpha^A_{xy}-\alpha^A_{yx}$, where $\alpha^A_{\rho\sigma}$ is the antisymmetric component of the polarizability [Eq. (5)].

Transition	Allowed polarization
$(\Gamma_4\Gamma_4)$	All polarizations allowed
$(\Gamma_4\Gamma_{5,6})$	(S_x, S_y), $(zx+xz,\ yz+zy)$, $(xx-yy,\ xy+yx)$
$(\Gamma_{5,6}\Gamma_{5,6})$	S_z, zz, $xx+yy$.

It should be remembered that the g factors were calculated to the accuracy allowed by the crystal field model, since we included J mixing within the ^4I term. The other mechanisms which might affect the g factors are an admixture of higher Russell–Saunders terms, covalency, and configuration interaction. A rough calculation of the matrix elements connecting the states of the ^4I and ^4F terms shows that their largest value is $(^4I|B^6_0C^{(6)}_0|^4F) \sim 5$ cm^{-1}. This is too small to bring about a significant correction of the g factors. The other two mechanisms could produce a change of about 10% in the g factors.[30,31] Birgeneau[31] showed that the ion-phonon interaction can contribute to the g factors. Substantial changes in the g factors from their values calculated on the basis of a static crystal field are expected in the extreme cases of resonance interaction between the phonons and the electronic levels. This has been observed[32] in the case of $NdCl_3$. We have reason to believe that the interaction with the phonons affects the g factors of the $^4I_{9/2}$ ground multiplet of $NdAlO_3$. The excited states of $^4I_{9/2}$ have energies within the phonon bands, so that a direct interaction could be important. Also, in the case of $PrAlO_3$ (and mixed crystals $Pr_xNd_{1-x}AlO_3$[33]) the interaction between the rare-earth ions and the phonons brings about phase transitions and substantially affects the electronic levels.

B. Electronic Raman Intensities

Selection rules for the electronic Raman effect were discussed in detail by Kiel and Porto.[34] Table V gives their results for the case of a paramagnetic ion with an odd number of electrons in D_3 symmetry, the site symmetry group of Nd^{3+} in this crystal. In our case the ground-state level is of Γ_4 symmetry type; at low temperature all the transitions will be from this level. Thus we expect to observe $\Gamma_4\rightarrow\Gamma_4$ transitions in all polarizations and $\Gamma_4\rightarrow\Gamma_{5,6}$ transitions in all but the zz polarizations. Therefore, we can use the zz polarization to distinguish between the two types of transitions. However, judging from Table I, which gives the relative intensities for phonon Raman scattering at room temperature and 2 °K, we observe that the polarization at 2 °K is incomplete. This can be seen for the Γ_3^+ phonon at 49 cm^{-1}, which is observed in zz polarization, and for the Γ_1^+ phonon at 251 cm^{-1}, which appears also in zy polarization. This depolarization effect is not due to crystal birefringence,[35] since the polarization was almost complete at room temperature. It should also be noted that the polarization observed in the absorption spectra was complete at all temperatures. Another possible source could be localized strains which occurred in the crystal during the cooling-down process, thus causing twinning.[11] However, examination of the crystal between cross polarizers showed no evidence of such an effect. We thus conclude that the partial polarization, which appears at low temperatures only, is somehow due to the influence of the electronic states of the Nd^{3+} ion.

In order to calculate the relative intensities for the electronic Raman scattering one has to know the ratio between the quantities α_1' and α_2' defined in Eq. (10). To a first approximation, considering only contributions from the excited $4f^25d$ configuration to the Raman transitions, this ratio is simply $\alpha_1'/\alpha_2'=\sqrt{\frac{5}{3}}\,h\nu/E_{5d}$. Putting $h\nu=20500$ cm^{-1} and $E_{5d}=42700$ cm^{-1} (calculated from the Faraday-rotation experiment[22]), we arrive at $\alpha_1'/\alpha_2'=0.62$. No agreement was found between the observed and calculated electronic Raman intensities when this value was used. Thus, the ratio α_1'/α_2' was taken as a variable parameter. The best agreement was found for $\alpha_1'/\alpha_2'=0.1$. The results for $^4I_{9/2}$ are summarized in Table VI. The $^4I_{11/2}$ was not used for the comparison between the calculated and measured intensities because the latter are unreliable due to the presence of fluorescence (see Sec. III). A qualitative agreement between measured and calculated intensities is observed. The discrepancies are as follows. The intensity of the $\Gamma_4^a\rightarrow\Gamma_4^b$ line at 122 cm^{-1} observed in zx polarization is about three times larger than the calculated one and the line at 595 cm^{-1} $(\Gamma_4^a\rightarrow\Gamma_4^c+\Gamma_{5,6}^b)$

TABLE VI. Calculated relative intensities of electronic Raman scattering in $NdAlO_3$. The observed intensities at 2 °K are given in parentheses. The intensities are normalized to that of the 122-cm^{-1} line in zz polarization (underlined).

Polarization → Energy (cm^{-1})	$xx(yy)$	zz	$xy(yx)$	$xz(yz)$	$zx(zy)$
122 (Γ_4^b)	34.7	<u>100.0</u> (<u>100.0</u>)	34.8 (41)	0.5 (5.5)	22.5 (77)
148 $(\Gamma_{5,6}^a)$	45.4	0 (5.5)	45.4 (45)	30.4 (46)	33.8 (42)
595 $(\Gamma_4^c+\Gamma_{5,6}^b)$	108	0.1 (16)	147.6 (38)	71.2 (29)	239.8 (78)

is observed in zz polarization where it is expected to have essentially zero intensity. This line appears in the other polarizations with intensity three times weaker than the calculated one.

There are two possible reasons for the lack of full agreement between the observed and calculated relative Raman intensities. The first has been mentioned above in discussing the g factors for the $^4I_{9/2}$ multiplet. The interaction between the states of this multiplet and the phonons mixes the eigenvectors of these two systems of excitations. This will affect the relative intensities of both electronic and phonon Raman lines. The other factor arises from the fact that the exciting laser line (4880 Å) lies very close to the excited ^2G and ^4G terms of Nd^{3+}. These multiplets are strongly connected to $^4I_{9/2}$ by the electric dipole matrix elements, as is evidence by the intense absorption in this region. Thus, the scattering process is one of near-resonance conditions and the relative intensities are altered. A detailed calculation of the resulting intensities is extremely difficult since the exact wave functions for the excited multiplets are required.

V. SUMMARY

In this study the crystal field model has been used in order to explain the energy-level scheme, the g factors, and the electronic Raman effect of $NdAlO_3$. It has been shown that the energy levels are well accounted for by the crystal field when J mixing within the ^4I term is included. Only qualitative agreement is obtained for the g factors and electronic Raman intensities. While one might expect large discrepancies between theory and experiment for the Raman intensities, the g factors only depend on the eigenvectors and should be as accurate as the crystal field model allows. Thus, it is concluded that the differences between the experimental and calculated g factors are due to the interaction with lattice vibrations which alters the eigenvectors. This also affects the relative Raman intensities. Another suggested source of error for the calculated intensities is the effect of excited levels (the ^2G and ^4G terms) within the $4f^3$ configuration, which are strongly connected to the ^4I term by the odd-parity components of the crystal field. In the case of the electronic Raman effect of $CeCl_3$ which was studied by Kiel *et al.*[4] a better agreement between calculated and experimental intensities was obtained. However, this system is simpler than the one studied here. The energy levels of the $4f^1$ configuration of Ce^{3+} spread over 2000 cm^{-1} and the only mechanisms which can produce electronic scattering are direct coupling to the even-parity configurations. A further study of the electronic Raman effect for rare-earth ions with complicated energy-level schemes in crystals is required for a better understanding of the scattering mechanisms.

ACKNOWLEDGMENTS

The authors wish to acknowledge the technical assistance of H. Katz. They are indebted to W. H. Grodkiewicz for growing the crystals used in this work.

APPENDIX

The transformation connecting the irreducible tensor components $\alpha_q^{(k)}$ with the Cartesian tensor components $\alpha_{\rho\sigma}$ is as follows:

$$\begin{aligned}
\alpha_{xx} &= \tfrac{1}{2}[\alpha_2^{(2)} + \alpha_{-2}^{(2)} - (2/\sqrt{3})\,\alpha_0^{(0)} - (2/\sqrt{6})\alpha_0^{(2)}]\,,\\
\alpha_{yy} &= \tfrac{1}{2}[\alpha_2^{(2)} + \alpha_{-2}^{(2)} + (2/\sqrt{3})\alpha_0^{(0)} + (2/\sqrt{6})\alpha_0^{(2)}]\,,\\
\alpha_{zz} &= (1/\sqrt{3})\,(-\alpha_0^{(0)} + \sqrt{2}\,\alpha_0^{(2)})\,,\\
\alpha_{xy} &= \tfrac{1}{2}\,i(\alpha_2^{(2)} - \alpha_{-2}^{(2)} + \sqrt{2}\,\alpha_0^{(1)})\,,\\
\alpha_{yx} &= -\tfrac{1}{2}\,i(\alpha_2^{(2)} - \alpha_{-2}^{(2)} - \sqrt{2}\,\alpha_0^{(1)})\,,\\
\alpha_{xz} &= -\tfrac{1}{2}(\alpha_1^{(1)} + \alpha_1^{(2)} + \alpha_{-1}^{(1)} - \alpha_{-1}^{(2)})\,,\\
\alpha_{zx} &= \tfrac{1}{2}(\alpha_1^{(1)} - \alpha_1^{(2)} + \alpha_{-1}^{(1)} + \alpha_{-1}^{(2)})\,,\\
\alpha_{yz} &= \tfrac{1}{2}\,i(\alpha_1^{(1)} + \alpha_1^{(2)} - \alpha_{-1}^{(1)} + \alpha_{-1}^{(2)})\,,\\
\alpha_{zy} &= -\tfrac{1}{2}\,i(\alpha_1^{(1)} - \alpha_1^{(2)} - \alpha_{-1}^{(1)} - \alpha_{-1}^{(2)})\,.
\end{aligned} \tag{A1}$$

$\alpha_0^{(0)} = 0$ for electronic Raman scattering and is included only for the sake of generality.

If the ground and excited states are crystal field levels, $|\psi) = \sum_{JM} a(JM)\,|\gamma JM)$, then

$$(\alpha_q^{(k)})_{gf} = \alpha_k'(\nu) \sum_{JMJ'M'} a^*(J'M')a(JM)\,(-1)^{J-M} \times \begin{pmatrix} J & k & J' \\ -M & q & M' \end{pmatrix} (\gamma SLJ \| U^{(k)} \| \gamma SLJ')\,, \tag{A2}$$

assuming that we are working within a given term. $\alpha_k'(\nu)$ is defined in Eq. (10). In the case of an odd number of electrons, symmetry properties lead to

$$|(\alpha_q^{(k)})_{gf}| = |(\alpha_{-q}^{(k)})_{g'f'}|\,, \tag{A3}$$

where g' and f' are the Kramers conjugate states of g and f. The intensities for a given polarization will be proportional to

$$|\alpha_{\rho\sigma}|^2 = \sum_{gf} |(\alpha_{\rho\sigma})_{gf}|^2\,, \tag{A4}$$

where $\rho, \sigma = x, y, z$ and the summation is over the degenerate states of g and f for a given transition. With the aid of Eqs. (A1) for the case of trigonal symmetry, i.e., $\Delta M = q (\mathrm{mod}\ 3)$, we obtain the following results (the indices f and g were suppressed):

$$\begin{aligned}
|\alpha_{xx}|^2 &= |\alpha_{yy}|^2 = \tfrac{1}{2}|\alpha_2^{(2)}|^2 + \tfrac{1}{3}|\alpha_0^{(2)}|^2\,,\\
|\alpha_{zz}|^2 &= \tfrac{4}{3}|\alpha_0^{(2)}|^2\,,\\
|\alpha_{xy}|^2 &= |\alpha_{yx}|^2 = \tfrac{1}{2}|\alpha_2^{(2)}|^2 + |\alpha_0^{(1)}|^2\,,
\end{aligned}$$

$$|\alpha_{xz}|^2 = |\alpha_{yz}|^2 = \tfrac{1}{2}|\alpha_1^{(2)} + \alpha_1^{(1)}|^2 ,$$

$$|\alpha_{zx}|^2 = |\alpha_{zy}|^2 = \tfrac{1}{2}|\alpha_1^{(2)} - \alpha_1^{(1)}|^2 . \quad \text{(A5)}$$

Each $\alpha_{\rho\sigma}$ in Eqs. (A5) corresponds to a given transition between the states f and g when the summation over the Kramers degenerate states has been carried out. In the case of accidental degeneracy, these expressions must be summed over each constituent state.

†Work supported in part by the Volkswagen Foundation.

*Present address: Division of Engineering, Brown University, Providence, R.I. 02912.

[1]J. D. Axe Jr., Phys. Rev. 136, A42 (1964).

[2]O. S. Mortensen and J. A. Koningstein, J. Chem. Phys. **48**, 3971 (1968).

[3]J. A. Koningstein and O. S. Mortensen, Phys. Rev. **168**, 75 (1968).

[4]A. Kiel, T. Damen, S. P. S. Porto, S. Singh, and F. Varsanyi, Phys. Rev. **178**, 1518 (1969).

[5]R. L. Wadsac, J. L. Lewis, B. E. Argyle, and R. K. Chang, Phys. Rev. B 3, 4342 (1971).

[6]R. T. Harley, W. Hayes, and S. R. P. Smith, in *Proceedings of the Second International Conference on Light Scattering in Solids,* edited by M. Balkanski (Flammarion, Paris, 1971), p. 357.

[7]S. Geller and V. B. Bala, Acta Crystallogr. **9**, 1019 (1956).

[8]Y. S. Kim, Acta Crystallogr. B **24**, 295 (1968).

[9]K. A. Müller, W. Berlinger, and F. Waldner, Phys. Rev. Lett. **21**, 284 (1968).

[10]J. F. Scott, Phys. Rev. **183**, 823 (1969).

[11]M. Marezio, P. D. Dernicz, and J. P. Remeika, J. Solid State Chem. **4**, 11 (1972).

[12]E. Cohen, L. A. Riseberg, W. A. Nordland, R. D. Burbank, R. C. Sherwood, and L. G. Van Uitert, Phys. Rev. **186**, 476 (1969).

[13]L. A. Riseberg, E. Cohen, W. A. Nordland, and L. G. Van Uitert, Phys. Lett. A **30**, 4 (1969).

[14]E. Finkman, E. Cohen, and L. G. Van Uitert, in Ref. 6, p. 369.

[15]G. F. Koster, J. O. Dimmock, R. G. Wheeler, and H. Statz, *Properties of the Thirty-Two Point Groups* (MIT, Cambridge, Mass., 1963).

[16]B. G. Wybourne, *Spectroscopic Properties of Rare Earths* (Interscience, New York, 1965).

[17]C. W. Nielson and G. F. Koster, *Spectroscopic Coeffcients for the p^n, d^n, and f^n Configurations* (MIT, Cambridge, Mass., 1964).

[18]B. R. Judd, Phys. Rev. **127**, 750 (1962).

[19]G. S. Ofelt, J. Chem. Phys. **37**, 511 (1962).

[20]B. R. Judd, Proc. R. Soc. A **250**, 562 (1959).

[21]K. Rajnak, J. Chem. Phys. **37**, 2440 (1962).

[22]C. R. Staton and W. H. Grodkiewicz, Faraday Rotation, Index of Refraction and Birefringence Measurement for $NdAlO_3$, Bell Laboratories Technical Memorandum, 1968 (unpublished).

[23]It should be noted that two of the lines (at 82 and 342 cm^{-1}) previously reported in Ref. 14 were erroneously identified. They were fluorescence lines.

[24]P. A. Fleury and S. P. S. Porto, J. Appl. Phys. **39**, 1035 (1968).

[25]R. London, Adv. Phys. **13**, 423 (1964).

[26]P. Alain and B. Piriou, Phys. Status Solidi B **43**, 669 (1971).

[27]M. T. Hutchings, in *Solid State Physics,* edited by F. Seitz and D. Turnbull (Academic, New York, 1964), Vol. 16.

[28]MINCON (D505) and MINUIT (D506), CERN 6600 Computer Program Library.

[29]N. Karayianis, J. Phys. Chem. Solids **32**, 2385 (1971); D. E. Wortman, J. Phys. Chem. Solids **33**, 311 (1972).

[30]M. Inoue, Phys. Rev. Lett. **11**, 196 (1963).

[31]R. J. Birgeneau, Phys. Rev. Lett. **19**, 160 (1967).

[32]E. Cohen, L. A. Riseberg, and H. W. Moos, Phys. Rev. **175**, 521 (1968).

[33]W. A. Nordland and L. G. Van Uitert, J. Phys. Chem. Solids **31**, 1257 (1970).

[34]A. Kiel and S. P. S. Porto, J. Mol. Spectrosc. **32**, 458 (1969).

[35]S. P. S. Porto, J. A. Giordamaine, and T. G. Damen, Phys. Rev. **147**, 608 (1966).